Available online at www.sciencedirect.com
SCIENCE DIRECT®

Journal of the European Ceramic Society 24 (2004) 3307–3315

www.elsevier.com/locate/jeurceramsoc

Creep behavior of a carbon-derived Si_3N_4/SiC nanocomposite

J. Dusza[a], J. Kovalčík[a], P. Hvizdoš[a], P. Šajgalík[b,*], M. Hnatko[b], M. Reece[c]

[a]*Institute of Materials Research, Slovak Academy of Sciences, Watsonova 47, Košice, Slovakia*
[b]*Institute of Inorganic Chemistry, Slovak Academy of Sciences, Dúbravská cesta 9, Bratislava 84536, Slovakia*
[c]*Queen Mary, University of London, Mile End Road, London, UK*

Abstract

The creep behavior of a silicon nitride–silicon carbide nanocomposite prepared by in situ utilizing $C + SiO_2$ carbothermal reduction is investigated at the temperature from 1200 to 1450 °C in bending with stresses ranking from 50 to 150 MPa in air. The stress exponents are in the interval from 0.8 to 1.28 and the apparent activation energy is 480 kJ/mol. No cavitation was found and grain-boundary sliding accommodated by diffusion through the intergranular glassy phase is considered to be the main creep mechanisms. The higher creep resistance of the nanocomposite compared with the creep resistance of a monolithic silicon nitride with the same amount of sintering additive can be explained by the presence of the intergranularly located SiC nano particles which limit grain boundary sliding and improve viscosity of the intergranular phase due to its changed chemical composition.

Keywords: Carbothermal reduction; Creep; Nanocomposites; Si_3N_4/SiC

1. Introduction

Silicon nitride-based ceramics are promising candidates for structural applications at temperatures higher than those allowed by metallic superalloys. However, their suitability to particular application as energy conversion systems, parts of engines and turbines, depends on their high temperature mechanical properties which are intimately linked to their microstructure and mainly to the amount and nature of sintering additives and the amount and properties of secondary phase.[1,2] Much effort has been made to optimize the type and volume fraction of the additive ($Al_2O_3 + Y_2O_3$, Y_2O_3 and Yb_2O_3) which is suitable for densification and at the same time exhibits high refractoriness as a grain boundary. Yttria and Ytterbia have been found most refractory at high temperatures and are preferred for applications such as advanced gas turbine engines. Crystallization of the grain boundary phase by heat treatment after the densification is another possible way to improve its refractoriness.[3–5] However, this method sometimes results in decreasing room temperature fracture toughness and strength. Another method to increase the strength of silicon nitride-based ceramics at high temperatures is to disperse crystalline particles (e.g. SiC) with high refractoriness at the grain boundaries.[6] Attention has to be paid, however, not to introduce microcracks, caused by the different thermal expansion coefficients of the particles and the matrix, into the material. To minimize or avoid microcrack formation, particles with very small size should be used as a dispersoids.

In the turn of 90′s Niihara proposed the ceramic nanocomposite concept and demonstrated that silicon nitride matrix composites with a dispersion of nanosized SiC particles exhibit enhanced properties (strength, creep resistance) compared to monolithic silicon nitride.[7–9] This improvement should be strongly related to the change of microstructure and chemistry of the composites, such as grain size/morphology, the distribution of the SiC particles, and structure and chemistry of grain boundaries, phase boundaries and intergranular phases.

During recent years $Si_3N_4 + SiC$ nanocomposites have been developed using different concepts/processing techniques, characterized as regards their microstructure and room and high temperature mechanical properties.[10–17] Most of the $Si_3N_4 + SiC$ nanocomposites were prepared by hot pressing and the hindered densification due to the presence of SiC particles was overcome using higher densification temperature comparing with that for the monolilitic Si_3N_4. In the case of gas pressure sintering the densification problem was be

* Corresponding author. Tel.: +421-55-6338115; fax: +421-55-6337108.
E-mail address: dusza@imrnov.saske.sk (J. Dusza).

0955-2219/$ - see front matter © 2003 Elsevier Ltd. All rights reserved.
doi:10.1016/j.jeurceramsoc.2003.10.046

solved by using relatively large amount of sintering additives, e.g. mixtures of yttria and alumina or silica. Herrmann et al.[18] prepared $Si_3N_4 + SiC$ nanocomposite with excellent high temperature properties using gas pressure sintering and sintering additive Y_2O_3.

Recent investigations have shown that the microstructure and the high-temperature strength of $Si_3N_4^+$ SiC nano-composites is strongly influenced by the nucleation step of the nanoparticles before the densification and that the high-temperature strength was improved only when the SiC nanoparticles are located intergranularly.[19]

The microstructure and chemistry of grain boundaries and grain boundary phases in different Si_3N_4 ceramics have been investigated by high resolution transmission electron microscope (HREM) and/or analytical electron microscopy (AEM).[20] It has been shown that an amorphous intergranular phase always exists at grain boundaries and at triple junctions and that the amorphous film at the grain boundary has an equilibrium thickness in a given ceramics and depends only on the chemistry of the system (sintering additives impurities, SiO_2 layer on the starting powder, etc.)

Pan et al.[21] investigated the grain morphology, phase distribution, and the morphology and distribution of SiC particles in $Si_3N_4 + SiC$ nanocomposites by HREM and the structure of grain boundaries and phase boundaries by HREM/lattice image technique. It was shown that the thickness of amorphous film at Si_3N_4 grain boundaries varies in this material. An amorphous film was found on the Si_3N_4/SiC boundaries in the case where the two crystal parts posses a random orientation with respect to each other. On the other hand clean phase boundaries were observed in the case when the lattices of the two crystal components showed a special orientation relationship.

Recently Rouxel et al.[22] studied the temperature dependence of Young's modulus in Si_3N_4-based ceramics. By the increased temperature slow decrease in modulus was found which ends in the temperature range 1000–1200 °C with slopes ranking from –13 MPa $°C^{-1}$ for the high purity Si_3N_4 grade, to −9 MPa $°C^{-1}$ for ceramics with more than 6 vol.% of additives. Above 1150 °C a rapid softening regime is observed, with dE/dT between −90 and −258 MPa $°C^{-1}$ for the pure Si_3N_4 and Si_3N_4 + 10 vol.% glass, respectively. With higher the Y/Al ratio in the glassy phase or SiC content in the material higher transition temperature, and smaller softening rate above the transition range was found.

Rendtel et al.[23] investigated high temperature properties of a GPS and HP $Si_3N_4 + SiC$ nanoceramics in the range of 1400–1600 °C. The annealing of the as-sintered materials promotes crystallization of the intergranular glassy phase resulting in an increase in creep strength and resistance against subcritical crack growth.

In the present study, the creep behavior of a recently developed carbon-derived $Si_3N_4 + SiC$ nanocomposite was investigated.

2. Experimental

2.1. Material

The nanocomposite was prepared by the preparation steps illustrated in Fig. 1.[24] The starting mixture was homogenized in polyethylene bottle with Si_3N_4 spheres in isopropanol for 24 h. Dried starting mixtures were sieved through 25-μm sieve in order to eliminate the large hard agglomerates. Green discs with the diameter of 48 mm and 5 mm thick were die pressed under the pressure of 30 MPa. The green discs were then embedded into a BN powder bed and positioned into the graphite uniaxial die. Samples were hot-pressed under a specific heating regime, atmosphere and mechanical pressure regime at 1750 °C for 2 h, Fig. 2. Hot-pressed samples were cut to the bars of 3 mm×4 mm×45 mm and polished to the 1 μm final finish. Density was measured by mercury immersion method. Polished samples were etched in the Polaron plasma barrel etcher PT 7150.

With the aim to study the influence of the in situ introduced SiC nanoparticles on the creep behaviour of the silicon nitride material a monolithic silicon nitride has been prepared with the same volume fraction of Y_2O_3 additive and with the similar processing steps.

2.2. Characterization methods

The microstructure of the nanocomposite was characterized by X-ray difractometry (XRD) scanning electron microscopy (SEM) and TEM/HREM.

XRD analysis was carried out using Philips X-part difractometer equipped with a CuK_2 radiation source. Both as-sintered and crept samples were analyzed. Analyses of the diffraction patterns were performed by comparison with the data listed in the library of the reference spectra of the Joint committee on Powder Diffraction Standards.

Polished and plasma-etched sections of the bulk materials were examined in a SEM. To prevent surface charging during examination the samples were coated with a thin layer of gold.

For TEM examination discs with a diameter of 3 mm were cut out from the bulk materials and mechanically ground to a thickness of 100 μm. They were further thinned to about 20 μm by dimpling, followed by ion-milling until perforation. The specimens were coated with a thin layer of carbon to minimize charging under electron beam radiation.

The overall structural and chemical characterization of each specimen was carried out by conventional and

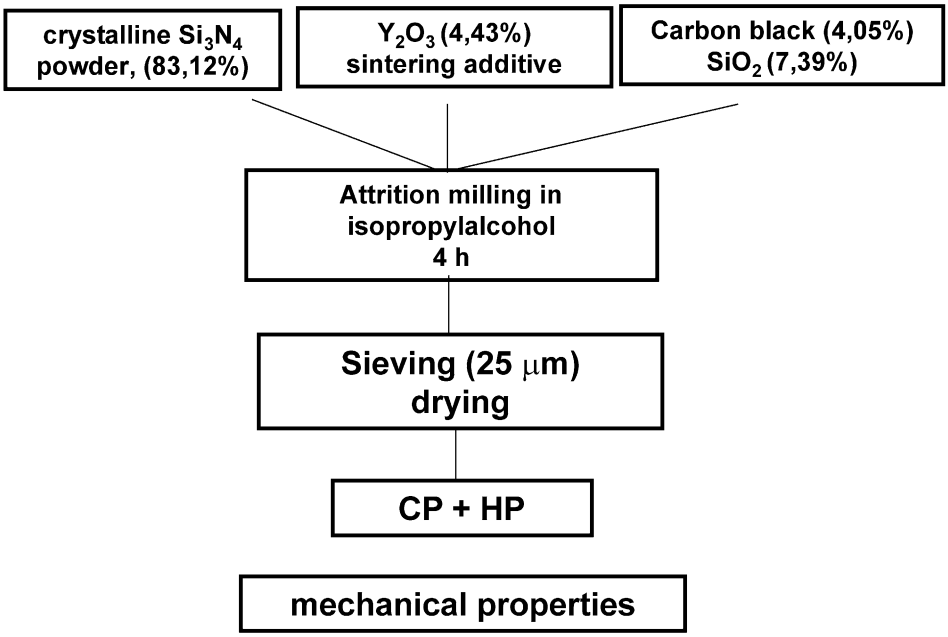

Fig. 1. Preparation steps of the carbon-derived nanocomposite.

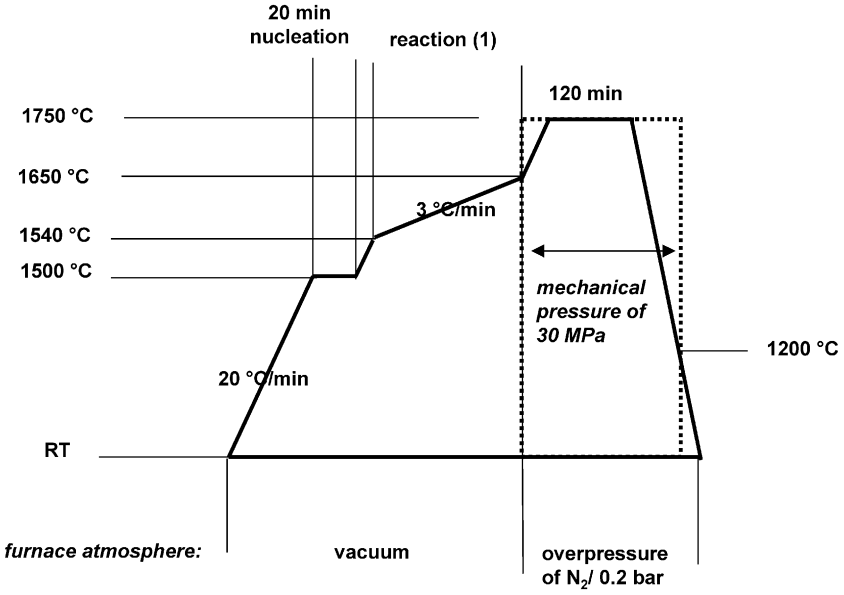

Fig. 2. Optimal processing regime for the preparation of the carbon-derived nanocomposite.

analytical TEM investigation with a Jeol-2010 microscope equipped with an ultra-thin window for energy-dispersive X-ray spectrometer. For structural analysis of grain boundaries and phase boundaries, as well as intergranular phase, the HREM lattice imaging technique was applied using a Jeol JEM-12000 microscope.

For testing the mechanical properties rectangular bars of the dimensions 3×4×45 mm were prepared. All specimens were ground with a 15 μm diamond wheel before testing. Edges were chamfered to eliminate machining defects.

The Young's modulus and internal friction of the investigated materials have been studied by impulse excited resonant vibration/damping analysis in the temperature range from 25 to 1400 °C.[25]

Creep tests were performed in four-point bending using a fixture made of silicon carbide with inner and outer span length of 20 and 40 mm, respectively. The measurements were carried out in a creep machine with dead-weight loading system in air atmosphere at temperature between 1200 °C and 1450 °C with outer fiber stresses in the range from 50 to 150 MPa. The sample

deflection was recorded continuously during the creep test. From the deflection data, the outer fibre strain was calculated as a function of time, t, by the method of Hollenberg et al.[26] and taken as the creep strain, ε. The creep rate was calculated from the slope of the ε versus t curve. The steady-state creep rate is usually described by the Norton equation:

$$\dot{\varepsilon} = A\sigma^n \frac{1}{\mathrm{d}^m} \exp\left(-\frac{Q_C}{RT}\right)$$

where A is a constant, depending on the respective material and on its microstructure, σ is the stress, n is the stress exponent, d is the grain size, m is the grain size exponent, Q_C is the activation energy for creep, and T and R have their usual meaning.

3. Results and discussion

Characteristic microstructures of the C-derived nanocomposite and monolithic Si_3N_4 is illustrated in the Fig. 3. The Si_3N_4 + SiC nanocomposite consists of a very fine, homogenously distributed Si_3N_4 grains with a low aspect ratio. The composite additionally contains globular nano and submicron-sized SiC particles, located intergranularly in the Si_3N_4 grains (average particle size approximately 30 nm) or intragranularly between the Si_3N_4 grains (average particle size approximately 150 nm). The intragranularly located SiC nanoparticles are easy to recognize on the etched ceramic section, but the intergranularly located SiC particles appear on the plasma etched surface in similar way as the intergranular phase and for their indentification TEM analysis was used.

The grain size (diameter) distribution of the Si_3N_4 grains in the nanocomposite is illustrated in Fig. 4. As it is visible the average Si_3N_4 grain size is below 150 nm and grains with diameter larger than 500 nm occurs in the microstructure only occasionally. No pores, cluster of grains/phases have been identified in the microstructure of the nanocomposite with only limited areas of free carbon with the maximum size of several micrometers.

The microstructure of the monolithic silicon nitride is slightly different in comparison to the composite material, Fig. 5. The average Si_3N_4 grain size is higher, between 150 nm and 500 nm with randomly present grains of a diameter up to 2 μm. Some micropores are present in the monolithic material with size from 0.1 to 1.0 μm. The distribution of the Si_3N_4 grains diameter in the monolithic material is illustrated in Fig. 6.

The main phase in both material is β-Si_3N_4 and a low amount of α-Si_3N_4. Beside the Si_3N_4 (and SiC in the composite) in both materials some additional crystalline phases have been detected which were mainly $YSiO_2N$ and $Y_2Si_3O_3N_4$. The volume fraction of these phases is

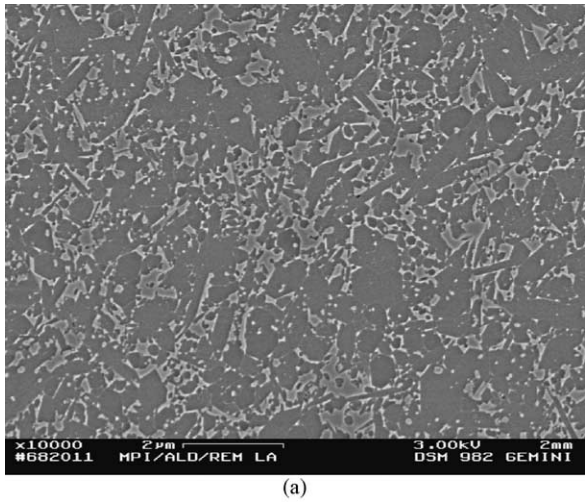

(a)

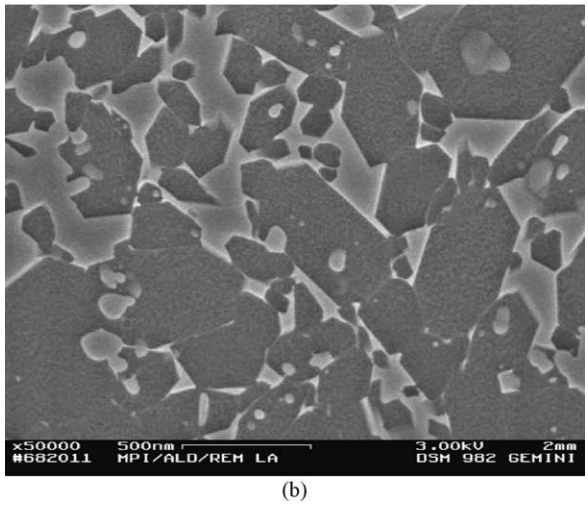

(b)

Fig. 3. Characteristic microstructure of the carbon-derived composite at lower (a) and high (b) magnification, SEM, plasma etched.

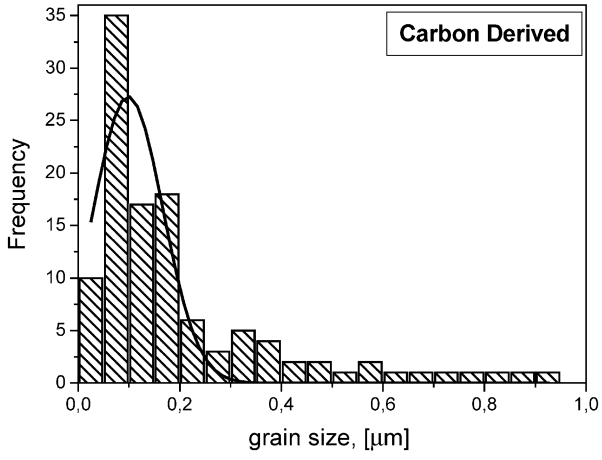

Fig. 4. Silicon nitride grain diameter distribution in the carbon-derived nanocomposite.

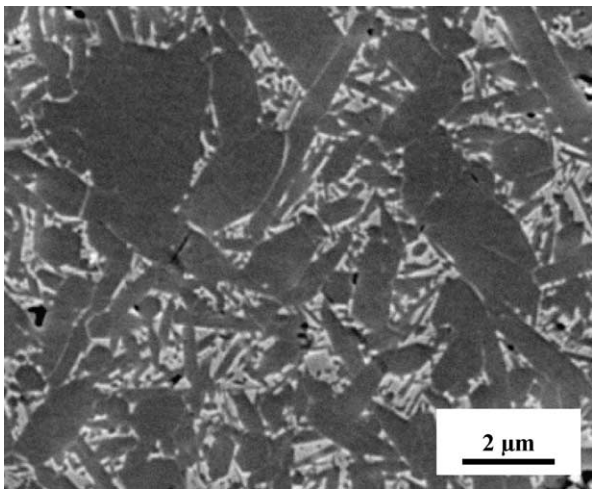

Fig. 5. Characteristic microstructure of the monolithic silicon nitride, SEM, plasma etched.

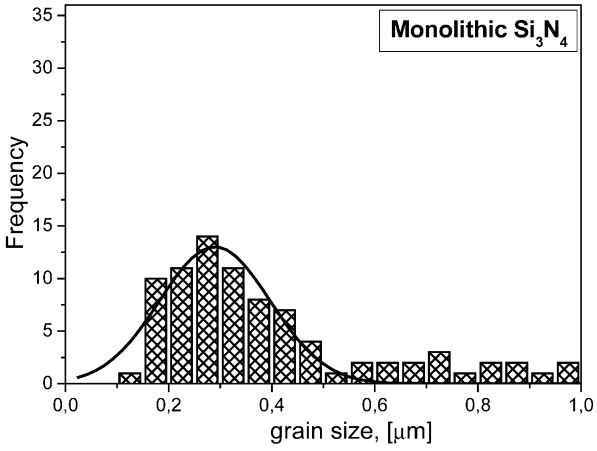

Fig. 6. Silicon nitride grain diameter distribution in the monolithic silicon nitride.

increasing during the creep test, mainly in the nanocomposite. It seems that during the creep the devitrification occurs rapidly, resulting in a near complete crystallization of the glass contained within the multigrain junction, but complete devitrification of the intergranular phase was not observed.

Characteristic microstructure of nanocomposite, prepared by TEM technique, are illustrated in the Figs. 7 and 8. In Fig. 7 shows intra and intergranularly located SiC nanoparticles in the microstructure of the composite material. As it is visible, the intergranularly located SiC nanoparticles are often interlocking the Si_3N_4/Si_3N_4 grains mainly in the case when their diameter is below of approximately 50 nm. In the case of intergranularly located SiC nanoparticles with a diameter comparable to the diameter of Si_3N_4 grains such an interlocking is not present, Fig. 8. TEM and HREM observations revealed that due to the intergranularly located SiC particles and crystallized glassy phase there are no glassy phase triple-points present in the microstructure of the

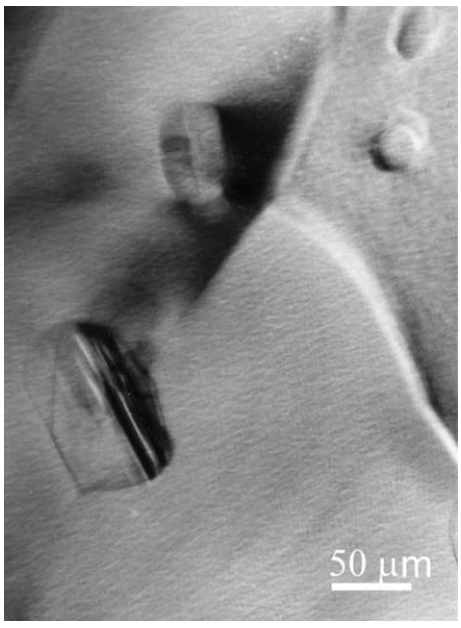

Fig. 7. Inter and intragranularly distributed SiC nanoparticles in the carbon-derived nanocomposite. Note the interlocked Si_3N_4 grains by the intergranulary located SiC particle—TEM.

composite, Fig. 9 and there is no equilibrium thickness of the intergranular phase between the Si_3N_4/Si_3N_4 grains and Si_3N_4/SiC grains. The average thickness of the intergranular glassy phase between the Si_3N_4/SiC is approximately 15A, Fig. 10, but in favorable orientation no boundary phase is present.

3.1. E-modulus and internal friction

Results of the impulse excited resonant vibration/damping analysis in the temperature range from 25 to 1400 °C show some differences between the behavior of nanocomposite and monolithic silicon nitride. The composite exhibits higher E-modulus in the whole testing range probably due to the present of SiC particles in the microstructure. Some changes in the microstructure have been detected at approximately 1075 °C during the heating-up of the composite probably connected with a crystallization of the part of the glassy phase, Fig. 11.

3.2. Creep rate

Characteristic creep curves of the nanocomposite, obtained in a step-wise loading regime are illustrated in Fig. 12. The creep deformation of both monolithic and composite ceramics can be characterized by a primary creep range and a pronounced steady-state creep range. Ternary creep regime was not observed in the studied materials at the used test conditions. From Fig. 12 it is evident that the composite ceramic exhibits minimum creep deformation up to 1300 °C. Significant creep deformation is detected at temperatures from 1350 to

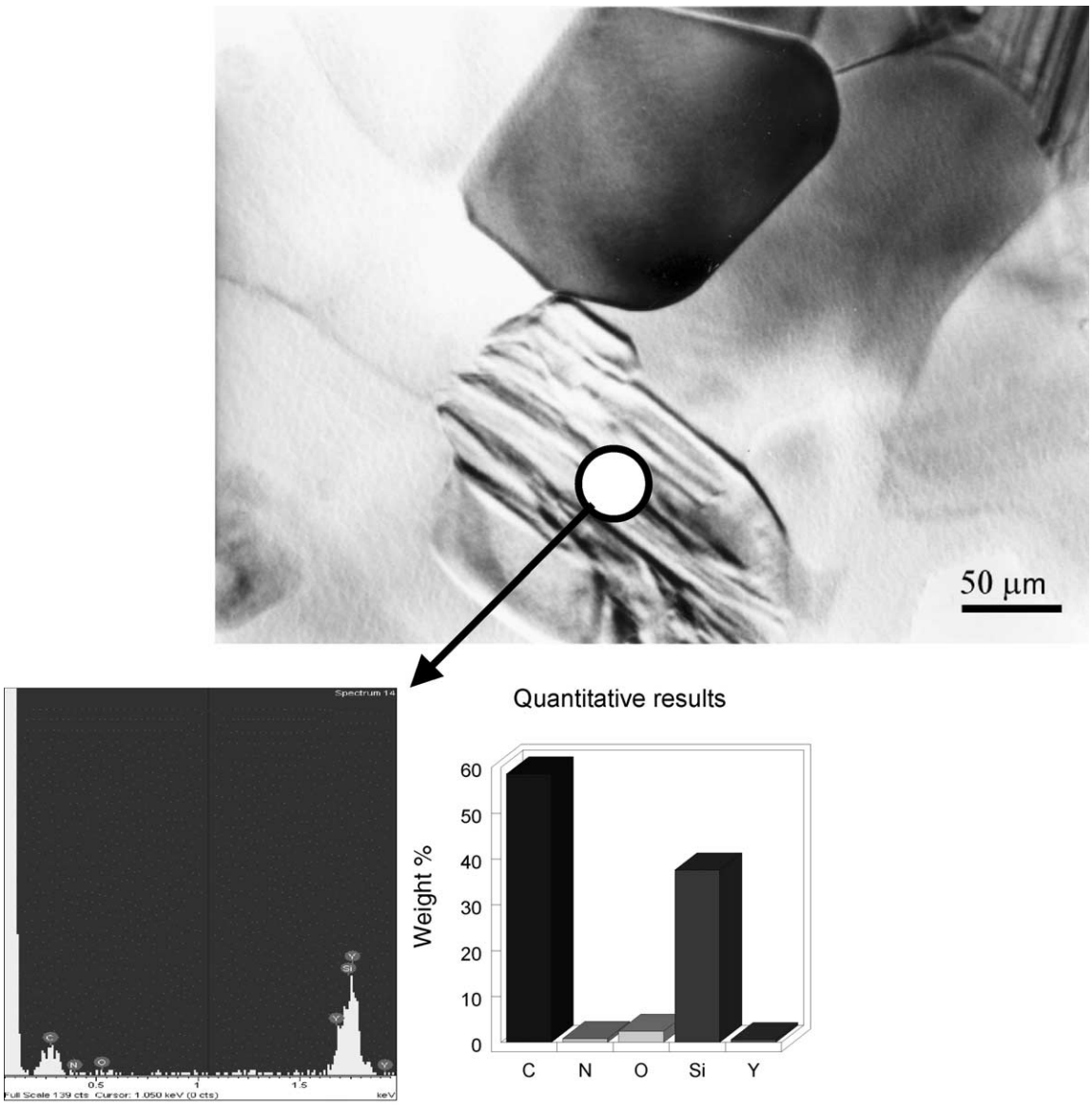

Fig. 8. Microstructure of the carbon-derived composite with the EDAX spectrum of a intergranularly located SiC particles.

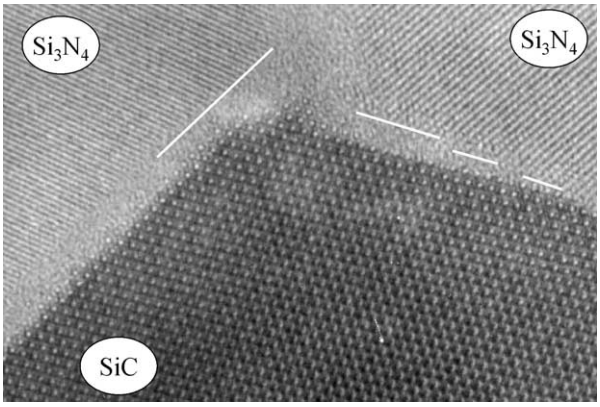

Fig. 9. Triple point and Si_3N_4/SiC grain boundaries in the carbon-derived compositewith different thickness of the intergranular phase between Si_3N_4 and SiC.

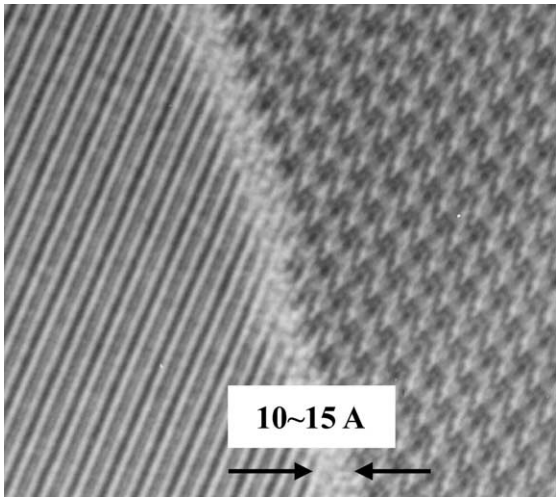

Fig. 10. Si_3N_4/SiC grain boundaries in the carbon- derived nano-composite.

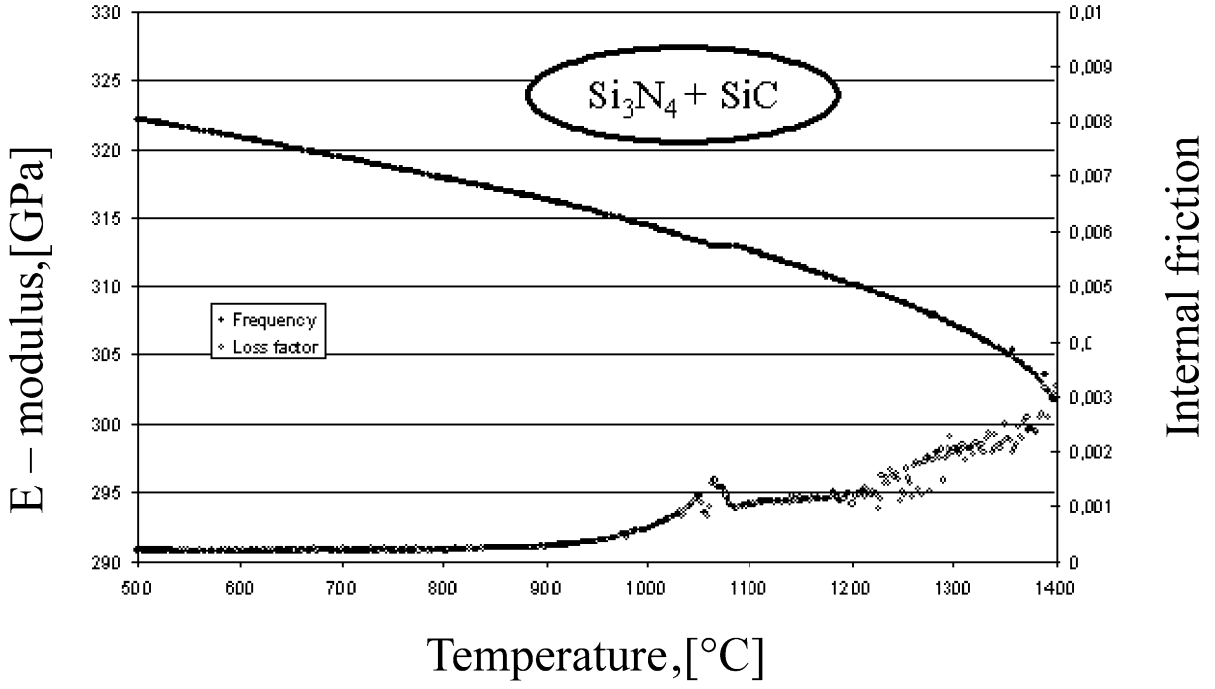

Fig. 11. Results of the impulse excited resonant vibration/damping analysis of nanocomposite.

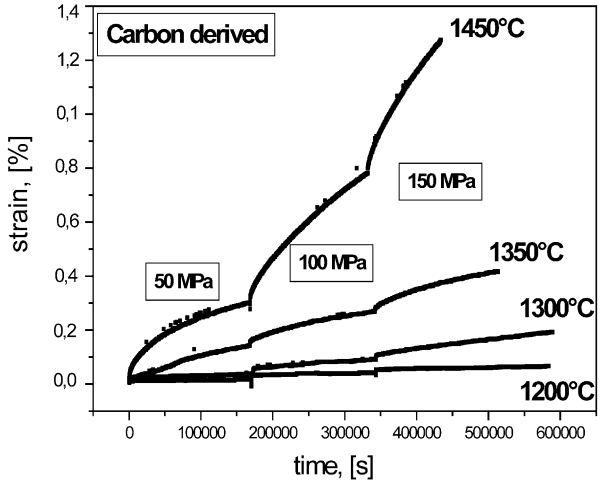

Fig. 12. Creep deformation at different temperatures and stresses.

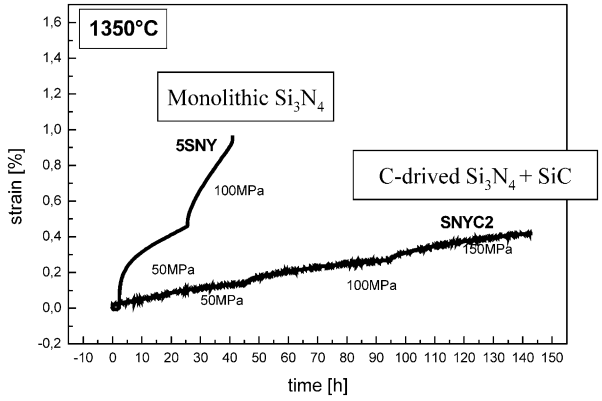

Fig. 13. Comparision of the creep deformation of monolithic silicon nitride and the C-derived nanocomposite.

1450 °C, only. The creep resistance of the nanocomposite was found to be significantly higher comparing to the creep resistance of the monolithic Si_3N_4. At the temperature of 1350 °C the composite exhibits similar creep strain at 150 MPa/150 h as the monolith at the condition of 50 MPa/25 h, Fig. 13.

3.3. Creep mechanisms—stress exponent

The influence of the applied stress on the creep rate of the nanocomposite at different temperatures is summarized in Fig. 14. The value of the stress exponent, n, was found in the temperature range from 1200 to 1450 °C at the applied stresses from 50 to 150 MPa in

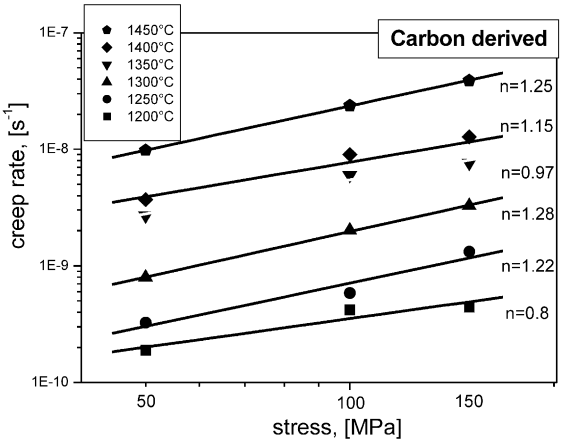

Fig. 14. Determination of the stress exponent of the C-derived nanocomposite.

the range from 0.8 to 1.28. A number of authors[27,28] reported a stress exponent about 1 at creep test of Si_3N_4 ceramics which contains low volume fraction of glassy phase. Such a low stress exponent is an indication that diffusion is the main creep mechanisms. Silicon nitride ceramics with a higher amount of the intergranular glassy phase exhibits a stress exponent of 2 or higher (in tests in tension) which is considered as a proof of presence of cavitation creep mechanism.[29] In the present investigation the stress exponent of the carbon-derived nanocomposite is close to unity, which indicates diffusional creep mechanisms. TEM observation of the crept specimens tested at the temperature of 1450 °C and 100 MPa revealed no sign of cavity formation in the composite during the test which supports the result of creep test and the above-mentioned consideration that the main creep mechanism is diffusion through the intergranular phase, probably connected with the solution/precipitation.

3.4. Creep mechanism—activation energy

The apparent activation energy of the carbon-derived nanocomposite for creep deformation determined from the creep rate under 100 MPa is 480 kJ/mol, Fig. 15. This value is higher than the activation energy of creep of monolithic Si_3N_4 and is comparable to the values of the activation energies of the creep of Si_3N_4+SiC nanocomposites prepared by addition of SiCN powder to the mixture.[28]

The activation energy of C-derived nanocomposite is close to the value of the thermal energy of solution of the silicon nitride in glassy phase (400 kJ/mol), measured from the densification experiment but proved by Menon et al.[30] and Wiederhorn et al.[31] This suggests that the creep deformation is controlled mainly by the solution of Si_3N_4 grains in the grain boundary phase. However, the slightly higher value of the creep activation energy (480 kJ/mol) comparing to this value suggests additional creep mechanisms. Todd and Xu.[32] reported approximately 700 kJ/mol for the activation energy for the diffusion of nitrogen ion through the grain boundary. Taking the values of the stress exponents into account we can conclude that the creep mechanisms in the C-derived nanocomposite are probably diffusion through the intergranular phase connected with the solution/precipitation and grain boundary sliding.

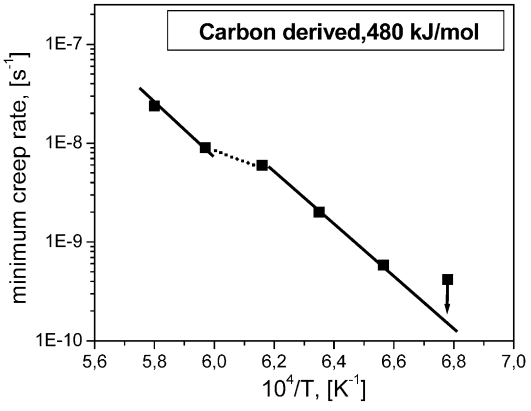

Fig. 15. Activation energy of the nanocomposite at the applied stress of 100 MPa.

4. Conclusions

The microstructure characteristics and creep behaviour of a carbon-derived Si_3N_4+SiC nanocomposite have been investigated. The main conclusions are the following:

- a defect-free material was fabricated using a cheap processing route;
- the material consists of submicron sized Si_3N_4 grains, inter/intragranularly located SiC nanoparticles and crystallized intergranular phase;
- the stress exponent and activation energy of creep in the temperature range from 1200 to 1450 °C under the stresses from 50 to 150 MPa were found to be approximately 1.1 and 480 kJ/mol, respectively;
- no cavitation was found trough TEM observation of the crep samples and the creep deformation is probably controlled mainly by solution-reprecipitation of the Si_3N_4 grains and grain boundary sliding.

Acknowledgements

This work was realized with the financial support of the Slovak Grant Agency, under the contract No. 2/1166/21 and by NANOSMART, Centre of Excellence, SAS. The authors acknowledge the help of G. Roebben, F. Phillipp and H. Labitzke.

References

1. Wang, C.-M., Pan, X., Hoffmann, M. J., Cannon, R. M. and Ruhle, M., Grain boundary films in rare-earth- glass-based silicon nitride. *J. Am. Ceram. Soc.*, 1996, **79**, 788–792.
2. Cinibulk, M. K., Thomas, G. and Johnson, S. M., Strength and creep behavior of rare-earth-disilcate-silicon nitride ceramics. *J. Am. Ceram. Soc.*, 1995, **75**, 2050–2055.
3. Bonnell, D. A., Tien, T.-Y. and Ruhle, M., Controlled crystallization of the amorphous phase in silicon nitride ceramics. *J. Am. Ceram. Soc.*, 1987, **70**, 460–465.
4. Cinibulk, M. K., Thomas, G. and Johnson, S. M., Grain- boundary -phase crystallization and strenght of silicon nitride sintered with YSiAlON glass. *J. Am. Ceram. Soc.*, 1990, **73**, 1606–1612.
5. Hoffmann, M. J., High temperature properties of Yb-containing Si_3N_4. In *Tailoring of Mechanical Properties of Si_3N_4 Ceramics*, ed. M. J. Hoffmann and G. Petzow. Kluwer, Dordrecht, 1993, pp. 233–244.

6. Lange, F. F., Effect of microsrtucture on strenght of Si_3N_4–SiC composite system. *J. Am. Ceram. Soc.*, 1973, **56**, 445–450.
7. Niihara, K., New design concept of structural ceramics–ceramic nanocomposites. *J. Ceram. Soc. Jpn.*, 1991, **99**, 974–982.
8. Hirano, T., Niihara, K., Ohji, T. and Wakai, F., Improved creep resistance of Si_3N_4/SiC nanocomposites fabricated from amorphous Si–C–A precursor powder. *J. Mater. Sci. Lett.*, 1996, **15**, 505–507.
9. Pezzoti, G. and Sakai, M., Effect of a silicon carbide nano-dispersion on the mechanical properties of silicon nitride. *J. Am. Ceram. Soc.*, 1994, **77**, 3039–3041.
10. Rendtel, A., Hübner, H., Herrmann, M. and Shubert, Ch., Si_3N_4/SiC nanocomposite materials: II, hot strength, creep, and oxidation resistance. *J. Am. Ceram. Soc.*, 1998, **81**, 1109–1120.
11. Klemm, H., Herrmann, M. and Schubert, Ch., High -temperature properties of Si_3N_4/SiC nanocomposites. *Ceram. Eng. Sci. Proc*, 2000, **21**(3), 713–720.
12. Rendtel, P., Rendtel, A. and Hübner, H., Mechanical properties of gas pressure sintered Si_3N_4/SiC nanocomposites. *J. Eur. Ceram. Soc.*, 2002, **22**, 2061–2070.
13. Besson, J.-L., Mayne, M., Bahloul-Hourlier, D. and Goursat, P., Si_3N_4/SiCN Nanocomposites: influence of SiC Nanoprecipitates on the Creep Behavior. *J. Eur. Ceram. Soc.*, 1998, **18**, 1893–1904.
14. Sternitzke, M., Review: Structural ceramic nanocomposites. *J. Eur. Ceram. Soc.*, 1997, **17**, 3259–3262.
15. Rouxel, T., Wakai, F. and Sakguchi, S., R-curve behavior and stable crack growth at elevated temperature (1500°–1650 °C) in a Si_3N_4/SiC nanocomposite. *J. Am. Ceram. Soc.*, 1994, **77**, 3237–3243.
16. Zhou, R., Feng, Z., Liang, Y., Zheng, F. and Xian, Q., Reactions between SiC and sintering aids in Si3N4/SiC nanocomposites and their concequences. *Ceram. Inter*, 2001, **27**, 571–576.
17. Dusza, J., Šajgalik, P., Steen, M. and Semerad, E., Low-cycle fatigue strength under step loading of a Si_3N_4 + SiC nanocomposite at 1350 °C. *J. Mater. Sci.*, 2001, **36**, 4469–4477.
18. Herrmann, M., Schubert, Ch., Rendtel, A. and Hübner, H., Si_3N_4/SiC nanocomposites materials: I fabrication and mechanical properties at room temperature. *J. Am. Ceram. Soc.*, 1998, **81**, 1095–1108.
19. Park, H., Kim, H. and Niihara, K., Microstructure and high-temperature strength of Si_3N_4–SiC nanocomposite. *J. Eur. Ceram. Soc.*, 1988, **18**, 907–914.
20. Kleebe, H.-J., Cinibulk, M. K., Tanaka, I., Bruley, J., Vetrano, J. S. and Rühle, M., High resolution electron microscopy studies on silicon nitride ceramics. In *Tailoring of Mechanical Properties of Si_3N_4 Ceramics*, ed. M. J. Hoffmann and G. Petzow. Kluwer, Academic Publisher, Dordrecht, The Netherlands, 1994, pp. 259–274.
21. Pan, X., Mayer, J. and Rühle, M., Silicon nitride based nanocomposite. *J. Am. Ceram. Soc.*, 1996, **79**, 585–590.
22. Rouxel, T., Youngs modulus and fracture of silicon nitride ceramics at elevated temperature. *Mat. Sci. Forum*, 2002, **383**, 3–12.
23. Rendtel, A. and Hüber, H., Effect of heat treatments on microstructure and creep behaviour of silicon nitride based ceramics. *J. Eur. Ceram. Soc.*, 2002, **22**, 2517–2525.
24. Hnatko, M. PhD Thesis, IIC SAS, Bratislava, 2002.
25. Roebben, G., Bollen, B., Brebels, A., Van, Humbeeck, J. and Van der Biest, O., Impulse excitation apparatus to measure resonant frequencies, elastic moduli and internal friction at room and high temperatures. *Rev. Sci. Instr.*, 1997, **68**, 4511–4515.
26. Hollemberg, G. W., Terwilliger, G. R. and Gordon, R. S., Calculation of stresses and strains in four-point bending creep tests. *J. Am. Ceram. Soc.*, 1971, **54**, 196–199.
27. Yoon, S.-Y., Akatsu, T. and Yasuda, E., The microstructure and creep deformation of hot-pressed Si_3N_4 with different amounts of sintering additives. *J. Mat. Res.*, 1996, **11**, 120–126.
28. Šajgalik, P., Hnatko, M., Lofaj, F., Hvizdos, P., Dusza, J., Warbichler, P., Hoffer, F., Riedel, R., Lecomte, E. and Hoffmann, M. J., SiC/Si_3N_4 Nano/micro-composite- processing, RT and HT mechanical properties. *J. Eur. Ceram. Soc.*, 2000, **20**, 453–462.
29. Lofaj, F., Usami, H., Okada, H. and Kawamoto, H., Creep damage in an advanced self-reinforced silicon nitride: Part I, cavitation in the amorphouse phase. *J. Am. Ceram. Soc.*, 1999, **82**, 1228–1234.
30. Menon, M. N., Fang, H. T., Wu, D. C., Jenkins, M. G. and Ferber, M. K., Creep and stress rupture behaviour of an advanced silicon nitride: Part II, creep rate behaviour. *J. Am. Ceram. Soc.*, 1994, **77**, 1228–1234.
31. Wiederhorn, S. M., Hockey, B. J., Crammer, D. C. and Yeckley, R., Transient creep behaviour of hot isostatically pressed silicon nitride. *J. Mater. Sci.*, 1993, **28**, 445–453.
32. Todd, J. A. and Xu, Z.-, The high-temperature Creep deformation of Si_3N_4–$6Y_2O_3$–$2Al_2O_3$. *J. Mater. Sci.*, 1993, **24**, 4443–4453.